ACS OMEGA

Open Access

http://pubs.acs.org/journal/acsodf

Article

Double-Layer Magnetic Microspheres with Dual Drug Delivery of Antibacterial and Maintenance Agents for the Treatment of *Candida albicans* Vaginitis

Haonan Li, Huijuan Huang, Sijia Xu, Hongmei Tian, Hui Xin, Xuan Zou, Ziquan Lv, Xiangjie Yao, Yinghua Xu,* Xiaobao Jin,* Shuiqing Gui,* and Xuemei Lu*

Cite This: *ACS Omega* 2025, 10, 11282−11295

Read Online

ACCESS | Metrics & More | Article Recommendations | Supporting Information

ABSTRACT: *Candida* vaginitis (CV) is the most common fungal infection among gynecological diseases, caused by *Candida albicans* (*C. albicans*). Traditional treatment for CV has led to increased antibiotic resistance, complicating treatment and indiscriminately killing both pathogens and beneficial bacteria in the vagina. Additionally, the inconvenience of traditional vaginal administration and the short residence time of treatments pose significant challenges. We developed a safe and effective combination drug delivery platform featuring magnetic bilayer gel microspheres to combine antibacterial properties and maintain the balance of the microbial community. This platform was characterized through a series of *in vitro* tests evaluating its dissolution, adherence, and retention properties, graded slow release, and antimicrobial effects. *In vivo* studies using CV mice models were conducted to assess antifungal properties, microecological regulation, magnetic residency, safety, and other related aspects. The results demonstrated that the material effectively inhibits the growth of *C. albicans*. It also increases the drug's residence time in the body and successfully releases probiotics, thereby improving vaginal microecology and promoting the recovery of inflammation to normal levels. These findings suggest a novel therapeutic approach for managing *C. albicans* vaginitis.

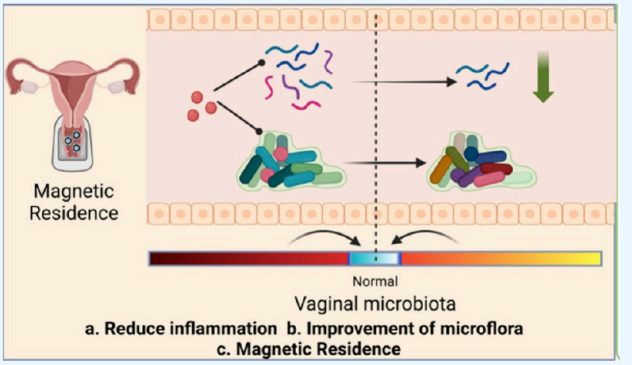

INTRODUCTION

Candida albicans (*C. albicans*) is one of the most common infectious causes of vaginitis and can occur in women of any age, particularly in women of childbearing age.[1,2] *C. albicans* is present in the vagina of approximately one-third of adult women and coexists with other microorganisms in the vagina without causing disease.[3,4] However, when changes occur in the internal environment, particularly when the vaginal pH increases, this disruption of the acidic environment compromises normal defense mechanisms. *Candida albicans* can then proliferate extensively and may transition into its hyphal form, enhancing its ability to adhere to and invade host tissues, thereby increasing its invasiveness and pathogenicity.[5] It has been reported that up to 75% of women of childbearing age are affected globally.[6] Traditional drug treatments rely on antibiotics, but resistance develops due to the misuse of these antibiotics, leading to increased recurrence rates.[7] Consequently, high infection rates among women and the rise in drug resistance have become urgent public health issues.

Currently, there is a growing focus on women's health, specifically the vaginal microbiome, which comprises a vast microecosystem containing billions of microorganisms and represents 9% of the total human microbiome.[8,9] The normal vaginal microbiota in women plays a crucial role in resisting the invasion of pathogenic bacteria by promoting and maintaining the stability of the microenvironment.[10,11] *Lactobacillus* species dominate the vaginal microbiota in healthy women. These bacteria maintain internal homeostasis and reduce the risk of disease by producing lactic acid and bacteriocins, which inhibit the growth of microorganisms associated with ecological imbalances.[12,13] Currently, probiotic supplements containing lactic acid bacteria are widely used to enhance immune function in the microecology.[14] The lactic acid and hydrogen peroxide produced by these supplements not only maintain a balanced microecology but also form a biological barrier, thereby protecting vaginal epithelial cells.[15,16]

Antimicrobial peptides (AMPs) are biologically active small molecules derived from various organisms and are a crucial

Received: December 5, 2024
Revised: March 1, 2025
Accepted: March 6, 2025
Published: March 12, 2025

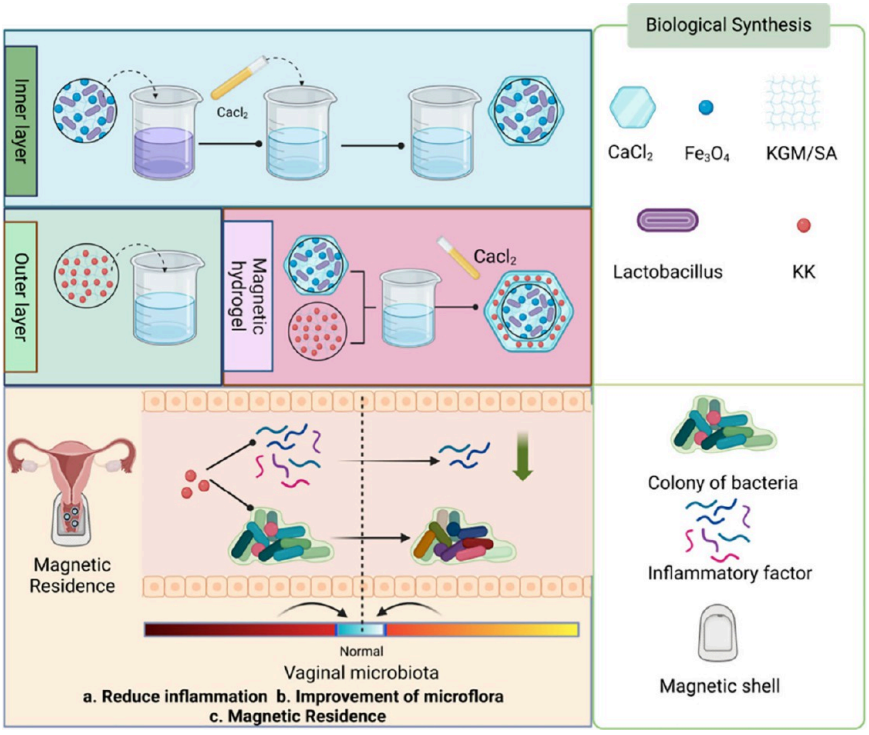

Figure 1. Preparation of double-layer magnetic microspheres loaded with drugs and probiotics and schematic diagram illustrating the treatment of vaginitis (created with BioRender.com).

component of innate immunity. AMPs are capable of disrupting bacterial biofilms, interfering with their metabolic pathways, and exerting potent antibacterial effects.[17,18] Small molecular weight antimicrobial peptides not only regulate the body's immune response but also exhibit potent antibacterial activity against a broad spectrum of microorganisms, including bacteria and fungi.[19,20] AMPs are considered safer alternatives to antibiotics, with a lower likelihood of developing resistance.[21] TetraF2W is known for its high antibacterial performance, low likelihood of resistance development, and reduced cytotoxicity. TetraF2W-KK is a short peptide derived from temporin-SHf, but research on its antibacterial effects and mechanisms, particularly against fungal infections like *C. albicans*, is currently limited.[22] Therefore, investigating the role of TetraF2W-KK in treating *C. albicans* vaginitis and expanding treatment options is important.[22−24]

Magnetic-driven hydrogel is composed of magnetic particles integrated with a hydrogel network. This hydrogel responds to and moves in response to externally applied magnetic fields, enabling drug release.[25,26] Magnetic nanoparticles offer unique advantages, including precise positioning control, rapid magnetic response, excellent controllability and drivability, and noninvasive remote operation.[27−29] Research has demonstrated that the hydrolysate of konjac glucomannan (KGM) supports the growth and metabolism of probiotics and has antibacterial properties, including those affecting *Lactobacillus* strains, thus supporting the potential application of KGM in vaginal health treatments. Additionally, with ongoing research, magnetic-driven hydrogels are increasingly applied in the field of biomedical materials, including magnetic-responsive drug delivery, magnetic resonance imaging, biosensing, and magnetic hyperthermia.[30−32] We propose that magnetically actuated hydrogels hold significant potential as therapeutic strategies for vaginitis.

In this study, to achieve a differential sustained-release function, we developed a magnetically resident double-layered gel microsphere drug delivery platform CS-K-L-GSMMS and investigated its therapeutic effects on CV using a mouse model including its anti-inflammatory, antibacterial, and regulatory effects on vaginal flora and related mechanisms As shown in Figure 1, the platform utilizes KGM and sodium alginate (SA) as the hydrogel matrix, with probiotics and magnetic materials encapsulated in the core and AMPs loaded in the outer layer.[33] By fixing the microspheres to the vaginal area using external magnetic patches, a sustained-release of AMPs and probiotics is achieved. Conventional local administration methods, such as metronidazole vaginal gel, have a shorter retention time in the vagina.[1] In contrast, this study can achieve magnetic retention by applying magnets to the affected area to maintain the microspheres in the tissue for an extended period. This combination achieves a differential sustained-release effect within the vagina, initially providing antifungal properties and subsequently releasing probiotics to regulate the vaginal microbiota, thereby developing a comprehensive treatment strategy that integrates antifungal efficacy with the maintenance of microbial balance. This will have significant practical significance for treating CV.

RESULTS AND DISCUSSION

Fe_3O_4@SiO_2 Particle Synthesis and CS-K-L-GSMMS Preparation and Characterization. To enhance the dispersion and homogeneity of Fe_3O_4 particles, Fe_3O_4@SiO_2 particles were prepared through the condensation reaction of TEOS.[34] Transmission electron microscopy results revealed that the synthesized Fe_3O_4@SiO_2 particles have a core−shell structure (Figure 2(a)). As shown in Figure 2(b−e), CS-K-L-GSMMS exhibited a complete, spherical structure with a relatively smooth surface (Figure 2(c)). Upon sectioning the

https://doi.org/10.1021/acsomega.4c11016
ACS Omega 2025, 10, 11282−11295

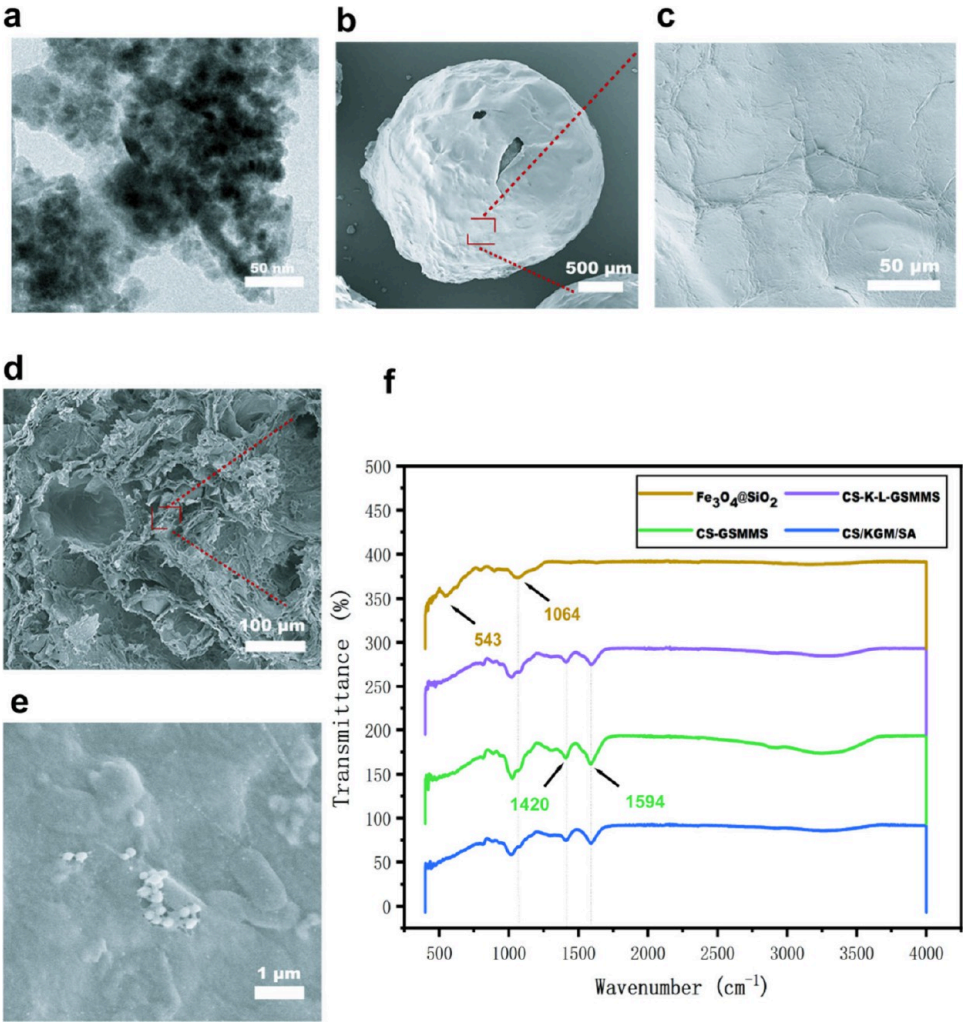

Figure 2. Preparation and characterization of a new multifunctional microsphere drug delivery platform CS-K-L-GSMMS. (a) TEM characterization of Fe_3O_4@SiO_2. (b, c) SEM are the overall and surface results of the microspheres, respectively. (d, e) SEM *Lactobacillus* inside the cross-section of microspheres and encapsulated lactobacilli, respectively. (f) Fourier infrared spectra of Fe_3O_4@SiO_2, CS-K-L-GSMMS, CS-GSMMS and CS/KGM/SA.

microspheres, numerous voids were observed in the cross-section and a reticular structure was visible internally (Figure 2(d)). According to previous research findings, the material exhibits an excellent delivery efficacy for probiotics.[35] Magnified views revealed *Lactobacillus* bacteria on the surface of the voids, indicating the successful encapsulation of probiotic bacteria (Figure 2(e)). This observation confirms that the probiotics were effectively encapsulated. Additionally, FT-IR was utilized to analyze the spectra of Fe_3O_4@SiO_2, CS-K-L-GSMMS, CS-GSMMS, and CS/KGM/SA. In the FT-IR spectrum of Fe_3O_4@SiO_2, characteristic peaks were observed at 543 cm^{-1} for the Fe−O group and a strong absorption band at 1064 cm^{-1}, corresponding to Si−O−Si bonding, confirming the successful synthesis of Fe_3O_4@SiO_2.[36] The spectra of CS-K-L-GSMMS, CS-GSMMS, and CS/KGM/SA showed asymmetric and symmetric stretching vibration peaks of the −COO group at 1420 and 1594 cm^{-1}. The lack of significant differences indicates that the addition of magnetic particles did not result in any migration of chemical bonds or affect the functionality of the microspheres (Figure 2(f)).

***In Vitro* Swelling Degradation and Drug Release of CS-K-L-GSMMS.** The swelling mechanism of CS-K-L-GSMMS in the SVF involves absorption and swelling until a complete rupture. In the SVF environment, the microspheres gradually swell and increase in water absorption, causing the internal structure of the hydrogel to become fluffy. As the swelling ratio increases, the release of the drug and *Lactobacillus* bacteria occurs at different rates. As depicted in Figure 3(a), the swelling ratio of the probiotic-loaded bilayer microspheres reached 8.35% after 8 h. After 24 h, the microspheres disintegrated due to excessive swelling and erosion. As shown in Figure 3(b), the release of *Lactobacillus* was slow for the first 10 h, with an increase in the release rate observed after 10 h, peaking at 18 h. The AMPs were released rapidly in a dose-dependent manner during the first 10 h, with a slower increase in release observed after 10 h. These results suggest that the time difference in the release of AMPs and probiotics creates a cascade release system for the treatment of CV. As shown in Figure 3(c), the cumulative release of AMPs was 60.83% after 24 h.

***In Vitro* Antibacterial Activity.** The drug-loaded microspheres exhibited bacteriostatic effects, as indicated by inhibition circles; a diameter of ≥ 10 mm is considered inhibitory according to Clinical and Laboratory Standards Institute (CLSI) standards, as shown in Figure 3(d). Furthermore, the drug-loaded microspheres were incubated with *C. albicans* to form a bactericidal curve, evaluating the

https://doi.org/10.1021/acsomega.4c11016
ACS Omega 2025, 10, 11282−11295

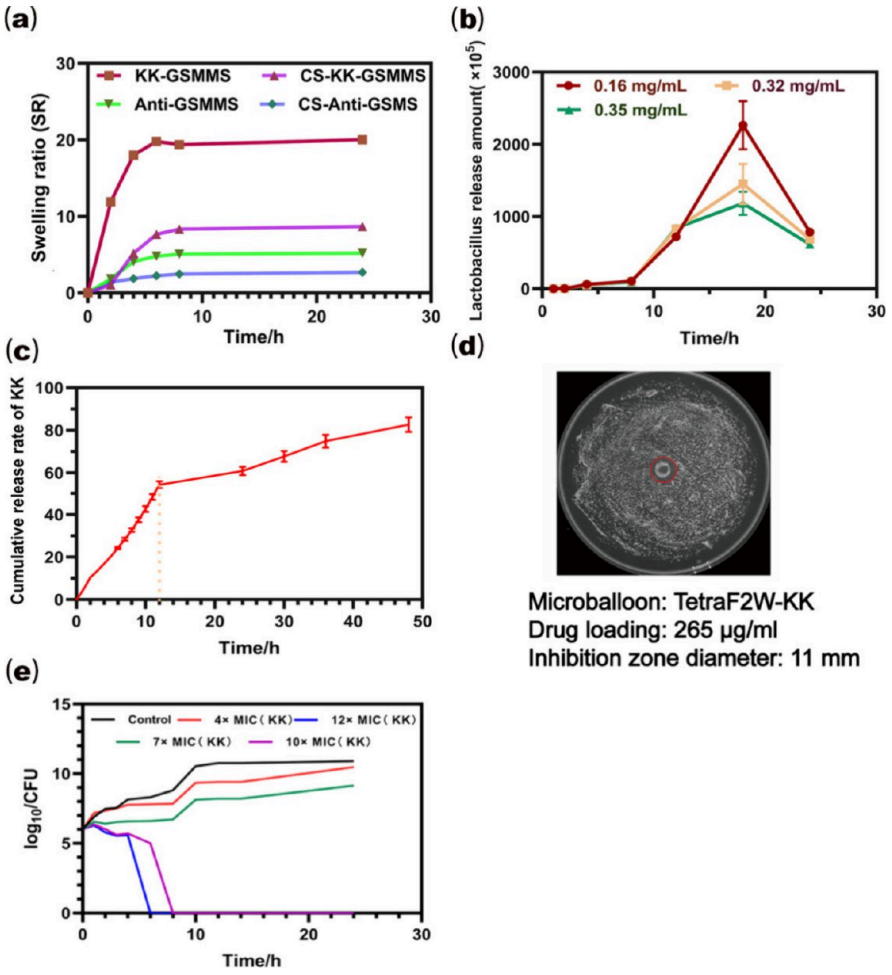

Figure 3. (a) Test of swelling ratio of single-layer, double-layer microspheres, and different drugs loaded in SVF; (b) cumulative release rates of probiotics; (c) cumulative release rates of antimicrobial peptides; (d) zone of inhibition (ZOI) test; (e) sterilization curve.

bactericidal effect of the drug-loaded microspheres. As depicted in Figure 3(e), when the drug concentration was >10 times the MIC value, the proliferation of *C. albicans* was rapidly inhibited, and no growth was observed after 8 h. This indicates that the drug released from the microspheres produced a bactericidal effect against *C. albicans*.

Evaluation of Adhesion Effect *In Vivo* and *In Vitro* on Vaginal Tissue. The *in vivo* imaging system was utilized to investigate the biological distribution of magnetic (CS-K-L-GSMMS) and nonmagnetic (CS-K-L-GSMS) materials at 0, 6, 12, and 24 h. As shown in Figure 4(a), no fluorescence was detected at 12 h when magnetic materials were not added to the microspheres. However, after the addition of magnetic materials, a strong fluorescence intensity was observed at 24 h under the effect of the external magnetic patch. This indicates that the incorporation of magnetic materials further prolonged the residence time of the microspheres in the vagina.

Furthermore, we also validated the adhesive properties of the materials *in vitro*. As shown in Figure 4(b), all microspheres demonstrated good mucosal adhesion properties, with three measurements of residency after 2 h recorded as 100%, 93%, and 96%, yielding an average value of 95%. This indicates that the double-layer microspheres enhanced adhesion and prolonged the duration of the intravaginal residency. After the addition of magnets, the remaining microspheres on the mucosal membrane were rinsed with SVF at a continuous flow rate of 9 mL/min. Despite rinsing, the remaining microspheres continued to adhere to the mucosa.

Assessment of the Efficacy of *In Vivo* Treatment for *Candida albicans* Vaginitis. First, we assessed the *Candida albicans* vaginitis model. As shown in Figure 5(a–c), vaginal secretions after modeling were observed under an electron microscope by using PAS staining and routine microscopy, revealing the presence of mycelia. Additionally, the fungus obtained by diluting the secretion and inoculating it on a selective culture plate turned green, confirming that *C. albicans* was present in the secretion. The fungus also appeared red and swollen after modeling, as shown in Figure 5(d), and the vulva became red and swollen postmodeling. These results indicate that the *C. albicans* vaginitis model was successfully established.

Furthermore, the efficacy of the treatment was validated through the assessment of changes in body weight and vulvar symptoms in mice post-treatment. As shown in Figure 5(f), before and after treatment, the body weight of mice in the control group was lower compared to those in other groups and exhibited a decreasing trend. In contrast, the treatment group gained different degrees of weight recovery. Observations of vulvar symptoms, shown in Figure 5(e), revealed that vulvar symptoms in the CS-K-L-GSMMS group were significantly reduced, like those in the normal group.

Reducing the prevalence of pathogenic bacteria and mitigating inflammatory responses within the vagina are

https://doi.org/10.1021/acsomega.4c11016
ACS Omega 2025, 10, 11282−11295

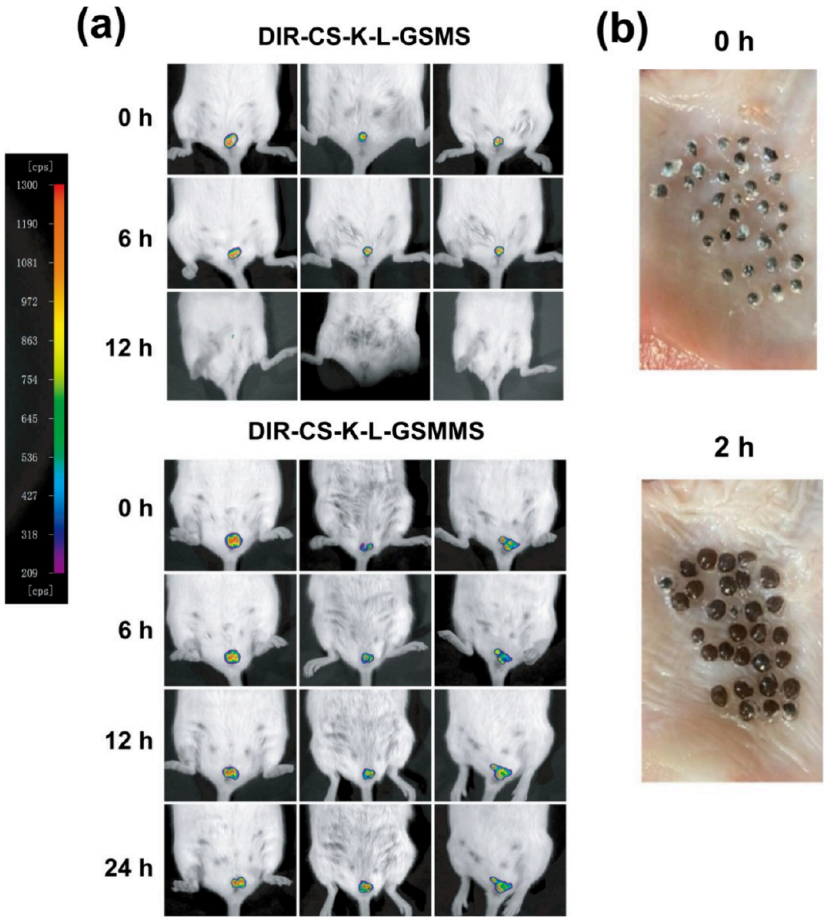

Figure 4. Investigation of retention time within and outside magnetic microspheres. (a) *In vivo* fluorescence results of fluorescent labeled magnetic material microspheres and blank magnetic free microspheres residing in the vagina at different time points. (b) *In vitro* adhesion and retention effects.

essential components in the management of *Candida albicans* vaginitis. As shown in Figure 6(a,b), there was no growth of *C. albicans* in the normal group. A substantial amount of bacterial growth was observed in the model and blank microsphere (MS) groups. The number of *C. albicans* was reduced to some extent in the TetraF2W-KK (KK) and *Lactobacillus* (Lab) groups, while only a few individual *C. albicans* growths were observed in the CS-K-L-GSMMS group and the Clotrimazole cream (CTR Cream) group. These results indicate that CS-K-L-GSMMS effectively inhibited fungal colonization.

As shown in Figure 7(a), after modeling, the levels of pro-inflammatory factors TNF-α, IL-1β, IL-6, MIP-2, and MCP-1 were significantly upregulated in mice, while the level of the anti-inflammatory factor IL-4 was downregulated. After CS-K-L-GSMMS treatment, the levels of TNF-α, IL-1β, IL-6, MIP-2, and MCP-1 were significantly decreased compared to those in the control group, and the IL-4 content was significantly increased. This indicates that CS-K-L-GSMMS effectively reduced the inflammatory response.

AS shown in Figure 7(b), Compared to the Control group, the mRNA expression levels of the pro-inflammatory factors TNF-α, IL-1β, and IL-6 in the control group were significantly upregulated, while the inflammation-suppressing factor IL-4 was downregulated. In comparison to the control group, the CS-K-L-GSMMS group exhibited significantly reduced mRNA levels associated with the pro-inflammatory factors TNF-α, IL-1β, and IL-6, and an elevated level of IL-4. These results were largely consistent with the ELISA assay findings.

Simultaneously, a histopathological examination of vaginal tissue was conducted. As shown in Figure 8(a), H&E staining of vaginal tissues revealed the following results: the normal group exhibited a complete tissue structure with intact mucosa. In contrast, the vaginal tissues of the control group and the MS group were damaged, with inflammatory infiltration and fungal colonization observed. The treatment group showed clear mucosal surface repair, an increase in mucosal thickness, and a substantial decrease in inflammatory infiltration.

After PAS staining, the mycelium or spores appeared purple, as indicated by the arrow in Figure 8b. In the Model and MS groups, many mycelia adhered to and were present in the vaginal lumen, with severe damage to the vaginal epithelial mucosa. In the CS-K-L-GSMMS and CTR Cream groups, significantly fewer adhering mycelia or spores were observed compared to the control group, indicating that CS-K-L-GSMMS significantly inhibited mycelial multiplication. Graphs displaying larger sizes of H&E and PAS staining results have been included in the Supporting Information Figure S1.

Analysis of Vaginal Flora Diversity by Vaginal Lavage in Mice. The vaginal microecology was restored to a healthy state through the introduction of *lactobacilli* into the vaginal environment. The relative abundance of vaginal microbial populations in mice after treatment was analyzed by using 16S rDNA sequencing. In cases of vaginal dysfunction, pathogenic bacteria such as *Proteus* and *Pseudomonas* tend to proliferate. This was analyzed by using the community composition bar graph, genus level, and species differences in the multiple group

https://doi.org/10.1021/acsomega.4c11016
ACS Omega 2025, 10, 11282−11295

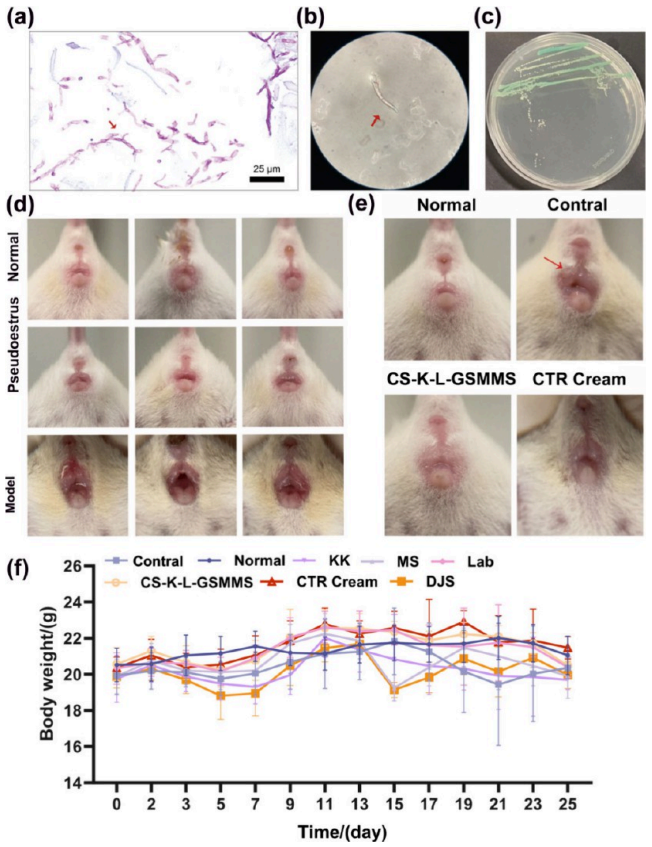

Figure 5. Modeling and therapeutic effect evaluation of *C. albicans* vaginitis. (a) Endoscopic examination of PAS staining secretions (40×); (b) Vaginal lavage fluid microscopic examination smear (40×); (c) Chromogenic culture medium to verify *C. albicans*; (d) Changes before and after external genitalia modeling. (e) Changes after external genital treatment. (f) Changes in physiological indicators of mice: Body weight change of rats;.

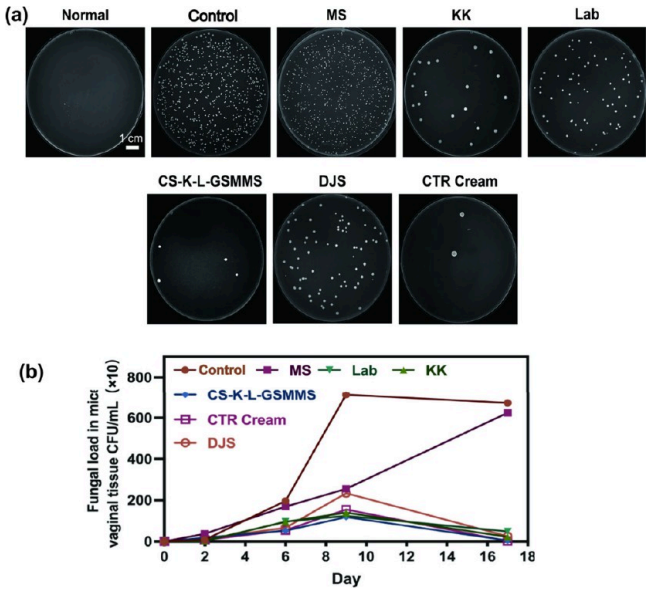

Figure 6. Evaluation of Antibacterial Efficacy *in vivo*. (a) Plate coating after treatment. (b) Fungal load count statistics during treatment.

difference test (Figure 9(a,b)). The results showed that the relative abundance of pathogenic bacterial genera significantly increased in the model after successful model construction. After treatment, the CS-K-L-GSMMS and CTR Cream groups exhibited significantly reduced relative abundances of *Proteus* and *Pseudomonas*. Additionally, the CS-K-L-GSMMS group showed a significant increase in the abundance of *Lactobacillus* after probiotic conditioning. Furthermore, the species-level analysis (Figure 10(a)) verified that the overall abundance of beneficial bacteria, such as *Staphylococcus* and *Lactobacillus*, increased in the treatment group, significantly improving the abundance of flora in CV mice. In summary, CS-K-L-GSMMS enhanced the abundance and diversity of beneficial bacteria in the vaginal microbiome, particularly *Lactobacillus*, and decreased the abundance of harmful bacteria, demonstrating its potential for the treatment and prevention of vaginal dysbiosis.

We observed that microbial levels vary between animals based on age, species, dominant genera, and phylum and genus levels. The mammalian vagina has a more taxonomically diverse bacterial spectrum, and the vaginal microenvironment and microbiota in animal models differ from those of human *C. albicans* vaginitis. Therefore, the relationship between rodent models and human disease warrants further investigation.

Circos analysis and species function prediction analysis (Figure 10(b,c)) indicated that the percentages of pathogenic bacteria *Proteus* and *Pseudomonas* in the control group were 27% and 56%, respectively. After treatment, these percentages were reduced to 15% and 7%, respectively, in the administered group. The percentage of *Lactobacillus* increased to 92% in the CS-K-L-GSMMS-treated group of mice. These results demonstrate a reduction in harmful microorganisms and an increase in the number and species of beneficial microbial populations in the treated group. Additionally, functional information and the abundance of microbial communities were predicted using the PICRUSt2 functional composition tool. The results showed significant differences in the expression of most pathways between the CS-K-L-GSMMS group and other groups except for some differences in the PWY-7663, PWY-7111, PWY-5101, ILEUSYN-PWY, VALSYN-PWY, and BRANCHED-CHAIN-AA-SYN-PWY pathways. This indicates that the treatment had a restorative effect on the vaginal microbiota.

***In Vivo* Safety Evaluation.** There was no significant difference in the organ indices of mice in the treatment groups at the end of treatment, as shown in Figure 11(a).

The results of heart staining showed that cardiomyocytes had clear transverse lines and centered nuclei, with a few blood vessels and connective tissues; in the liver, hepatocytes uniformly surrounded the central vein, forming a plate-like structure; in the spleen, there was a clear white medullary structure consisting of splenic vesicles and periarteriolar lymphatic sheaths, which was clearly differentiated from the red medulla; in the lungs, no obvious fat vacuoles were seen; the tissue texture was clear, and there was no angiofibrous hyperplasia; and the kidneys showed a complete glomerulus and peripheral tubules, with a clear overall structure. There were no obvious fat vacuoles in the lungs; the tissue texture was clear, and no vascular fibroplasia was observed. The tissues of the mice in the treatment group were intact with a clear texture and no obvious inflammation or lesions. Combined with the above results, CS-K-L-GSMMS did not produce any obvious abnormal responses in the main organs of the mice (Figure 11(b)). These results indicate that the developed magnetically responsive double-layer microsphere drug delivery system did not cause any damage or abnormalities to the organs.

The metabolic capacity of the liver and kidneys enables us to evaluate whether the material has toxic side effects on the body

https://doi.org/10.1021/acsomega.4c11016
ACS Omega 2025, 10, 11282−11295

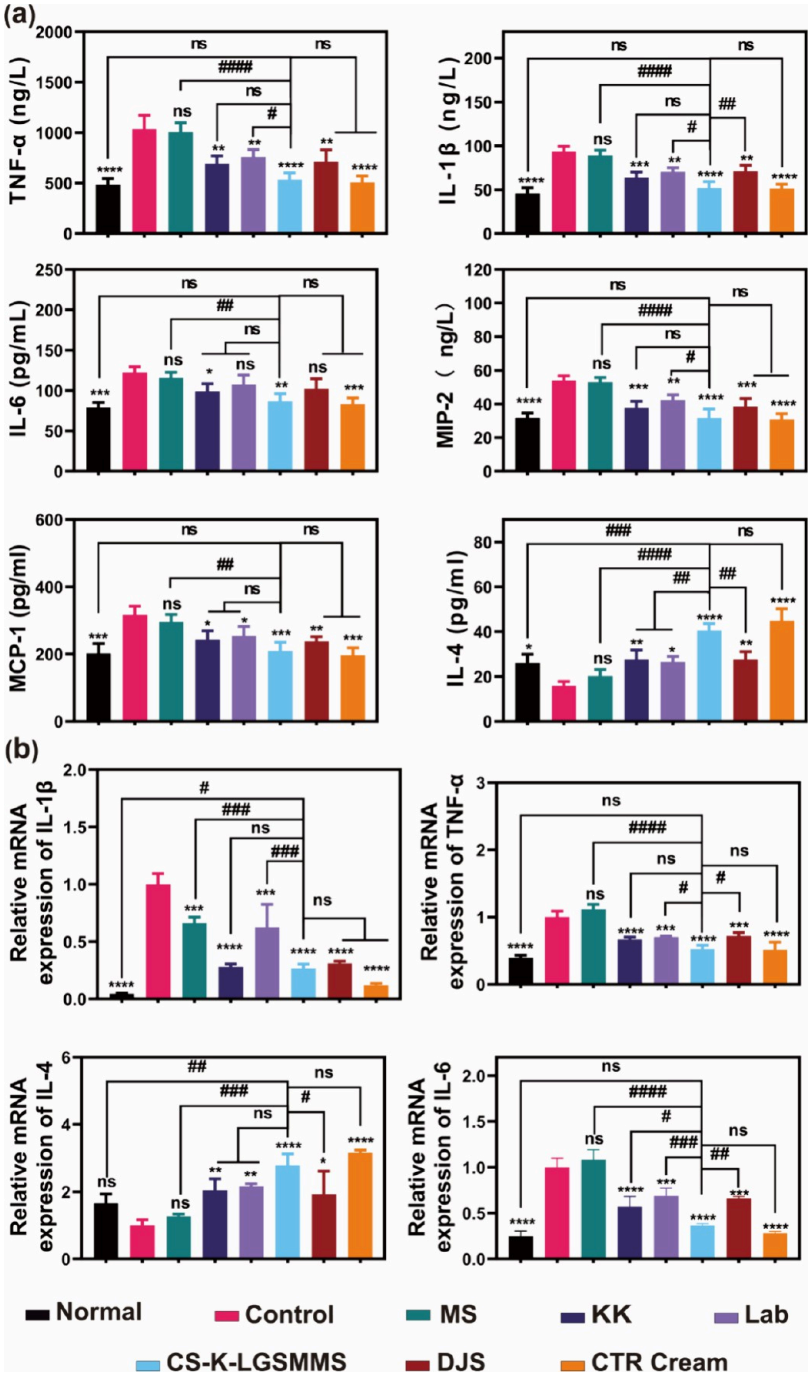

Figure 7. Evaluation of anti-inflammatory efficacy *in vivo*. (a) Concentrations of inflammatory markers in vaginal tissue. TNF-α, IL-1β, IL-6, MIP-2, MCP-1, and IL-4. (b) Expression of mRNA of inflammatory factor related genes: IL-1β, TNF-α, IL-4, and IL-6. *$p < 0.05$, **$p < 0.01$, ***$p < 0.001$, and ****$p < 0.0001$ compared to control group; $^{\#}p < 0.01$, $^{\#\#}p < 0.01$, $^{\#\#\#}p < 0.001$, $^{\text{and }\#\#\#\#}p < 0.0001$ compared to CS-K-L-GSMMS group, ns indicates no significant difference.

and thus verify its safety. As shown in Figure 11(c–f), the control group was superior to the normal group, but still within the normal range, and the rest of the groups were in the normal range of the effects on the indicators. There was no significant difference from the normal group, indicating that the liver and kidney functions of the mice were normal. This indicates that CS-K-L-GSMMS did not cause significant damage to the liver or kidney functions of the mice.

CONCLUSIONS

We designed a magnetically responsive dual-layer microsphere drug delivery platform, CS-K-L-GSMMS, which exhibited good swelling performance and release efficiency, antimicrobial properties, and adhesion effects and demonstrated excellent biocompatibility. The design is placed inside the vagina, and under the action of external magnets, it is continuously released to maintain a stable antimicrobial performance. Initially, it exerts antifungal effects for a certain period, followed by the release of probiotics to regulate the vaginal flora. CS-K-L-GSMMS

https://doi.org/10.1021/acsomega.4c11016
ACS Omega 2025, 10, 11282−11295

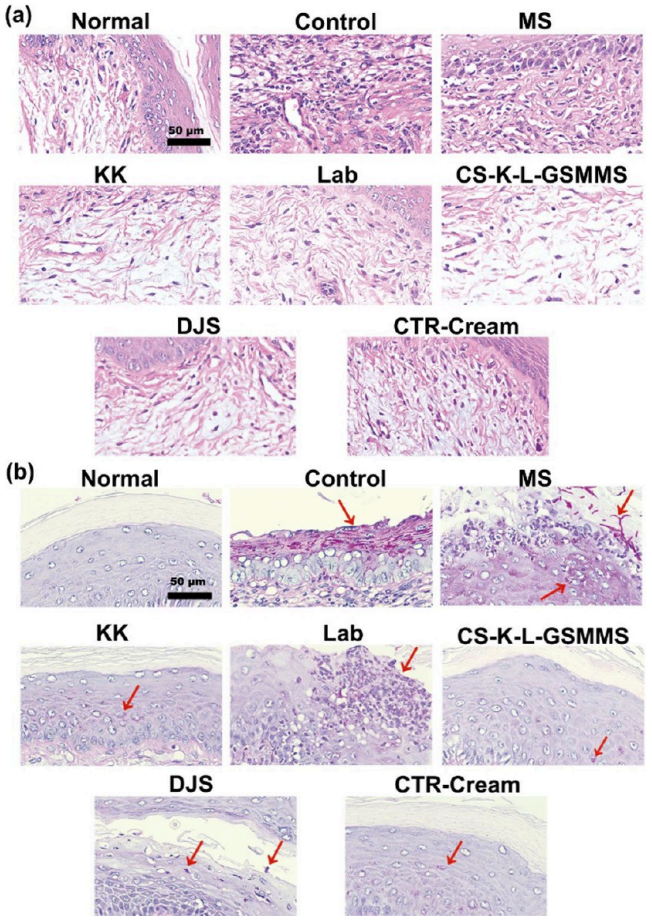

Figure 8. Histopathological changes in mice vaginal tissue. (a) H & E. (b) PAS. (The arrows indicate the presence of pathogenic bacteria.)

significantly inhibited *C. albicans* infection and improved vulvar redness and swelling, tissue pathological damage, and fungal infection damage. It has anti-inflammatory and antioxidant effects, improves the abundance of vaginal flora, and effectively regulates vaginal microecology. In conclusion, we designed a magnet-driven hydrogel microsphere that can provide both antimicrobial and vaginal microbiota-regulating effects, aiming to offer a research direction for the combined treatment of antifungal and maintenance therapies for *C. albicans* vaginitis.

MATERIAL AND METHODS

Materials. KGM was purchased from McLean Biochemistry. SA and nano ferric tetroxide were obtained from Aladdin Reagent Shanghai Co. Chitosan was acquired from Shanghai Yuanye Biotechnology Co. Pak Nien-selective medium was purchased from Guangdong Huankai Microbial Technology Co. ELISA kits were purchased from Jiangsu Enzyme Immunity Industry Co. Superoxide dismutase (SOD), catalase (CAT), malondialdehyde (MDA), aspartate aminotransferase (AST), alanine aminotransferase (ALT), blood urea nitrogen (BUN), and creatinine (CRE) assays were obtained from the Nanjing Jianjian Institute of Bioengineering (Nanjing, China). A hematoxylin and eosin (H&E) staining kit was purchased from Biyuntian Biotechnology Co., Ltd. Clotrimazole cream (CTR Cream) was purchased from Shanghai Second Pharmaceutical Co., Ltd. Each clotrimazole cream contains 10 mg of clotrimazole. Live *Lactobacillus* capsules for vaginal use (DJS) were purchased from Inner Mongolia Shuangqi Pharmaceutical Co., Ltd. The DJS were 0.25 g/capsule; each capsule containing live *Lactobacillus* should not be less than 2.5×10^5 CFU.

Synthetic Fe_3O_4@SiO_2. First, 1 g of Fe_3O_4 nanoparticles was weighed and ultrasonically dispersed in 100 mL of 80% ethanol. Then, 2 mL of tetraethyl orthosilicate (TEOS) were added while mixing, and ammonia was slowly added to adjust the pH to 10. The mixture was stirred at room temperature for 6 h and then vacuum-dried. Silica coatings were formed by the condensation of magnetite nanoparticles. The core−shell-structured Fe_3O_4@SiO_2 nanoparticles were collected using a magnet, washed several times with deionized water, and then dried before use.

Probiotic Preparation. *Lactobacillus fermentum, Lactobacillus acidophilus*, and *Lactobacillus teichneri* were adjusted to a concentration of 1.8×10^{10} CFU/mL by counting the colonies. Next, 1 mL of the mixed bacterial solution was extracted, and the bacteria were washed twice with sterile water before use in the microsphere preparation. The suspension was centrifuged at 3000 rpm for 5 min at 4 °C, and the supernatant was removed. The bacterial pellet was washed twice with sterile water before being used to prepare the microspheres.

Construction of CS-K-L-GSMMS. The processed *Lactobacillus* concentrate was combined with a KGM/SA mixed solution (10^{10} CFU/mL) in a biosafety cabinet and stirred well. Subsequently, 3% Fe_3O_4@SiO_2 was added, and the mixture was stirred. *Lactobacillus*-GSMMS was prepared by slowly dropping a 2% $CaCl_2$ solution into a 1 mL syringe (for the inner layer). A specific concentration of the AMP solution, dissolved in 10% of the total volume of a DMSO solution and then adjusted to a certain volume with sterile water, was mixed with the 3% KGM/SA solution. The KGM/SA was then diluted to 2% to fully encapsulate the previously prepared probiotic-containing microspheres. The microspheres were then placed in a 2% $CaCl_2$ solution for curing. After complete curing, the microspheres were washed three times, fully immersed in a 2% CS solution, and left to stand for 2 min to form a surface coating. After the microspheres were removed, they were washed three additional times and lyophilized for future use.

Characterization. The synthesized Fe_3O_4@SiO_2 particles were examined by using a transmission electron microscope (JEM2100, Japan). The morphology of the materials was examined using scanning electron microscopy (TESCAN MIRA LMS, Czech Republic). The samples were freeze-dried, ground into a powder, and mixed with potassium bromide. The mixture was pressed at a sample-to-potassium bromide ratio of 1:100. After treatment, the samples were tested and analyzed for structural information using Fourier transform infrared spectroscopy (FT-IR; Thermo Scientific Nicolet iS50, USA) in the scanning range of 4000−400 cm^{-1}. The data were mapped and analyzed by using Origin software. The samples were magnetized using a vibrating sample magnetometer (Lake Shore 7404, USA).

Evaluation of *In Vitro* Adhesion and Retention Effects. The porcine vaginal mucosa was obtained from a local abattoir, separated from the underlying tissue, and washed with phosphate buffer (pH 5.5). It was then sliced to a size of 40 × 25 mm and placed vertically in a constant temperature chamber at 37 °C. Next, 30 microspheres were gently pressed onto the tissue sections and subjected to a continuous flow (9 mL/min) of pH 5.5 phosphate buffer solution in the SVF to simulate physiological conditions. The mucosal adhesion capacity of the microspheres was monitored for 2 h and expressed as the

https://doi.org/10.1021/acsomega.4c11016
ACS Omega 2025, 10, 11282−11295

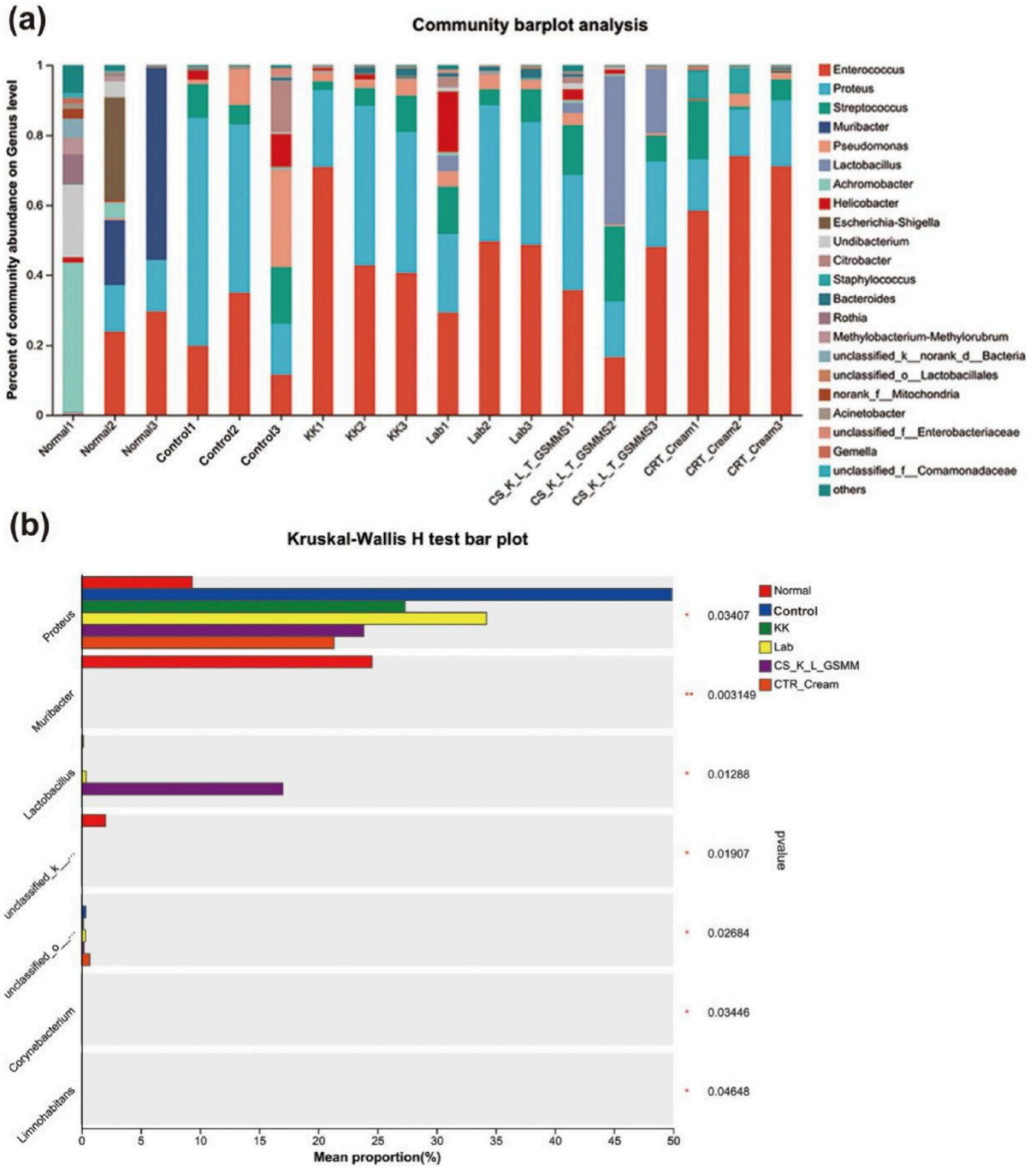

Figure 9. Microflora analysis after treatment with magnetic microspheres. (a) Percent of community abundance on the Genus level. (b) Kruskal–Wallis H test bar plot.

mucosal adhesion time and the percentage of microspheres remaining in the mucosa at the end of the experiment (average of three measurements).

Antibacterial Assays. (1) *Candida albicans* was used for the inhibition zone experiment. After administration, the drug spread on the plate and inhibited the growth of the surrounding bacteria, forming a transparent inhibition circle. The diameter of the inhibition zone was measured using a ruler, and the test was repeated three times to obtain an average value. (2) A single colony of *C. albicans* was grown in 5 mL of Yeast Malt Agar (YM) liquid medium for 18 h and then prepared for use. Drug-loaded microspheres were prepared in concentrations of 4 × minimum inhibitory concentration (MIC), 7 × MIC, 10 × MIC, and 12 × MIC. These were placed in 50 mL centrifuge tubes, and a tube without microspheres was marked as the control. Each tube received 10 mL of a 1640 culture medium. To prepare the suspension, 30 μL of *C. albicans* was added to 5 mL of culture medium, resulting in a final concentration of approximately 5 × 10^6 CFU/mL. Samples were collected at 0, 2, 4, 6, 8, 12, 16, and 24 h, diluted to a specific gradient for plating, and incubated at 28 °C. After 24 h of incubation, the samples were counted, and the experiment was repeated three times.

***In Vitro* Swelling Rate and Release Assay.** Swelling rate: Simulated vaginal fluid (SVF) was prepared and obtained, and its composition is shown in Table 1.[37] The different types of prepared microspheres were lyophilized at −50 °C and weighed

https://doi.org/10.1021/acsomega.4c11016
ACS Omega 2025, 10, 11282−11295

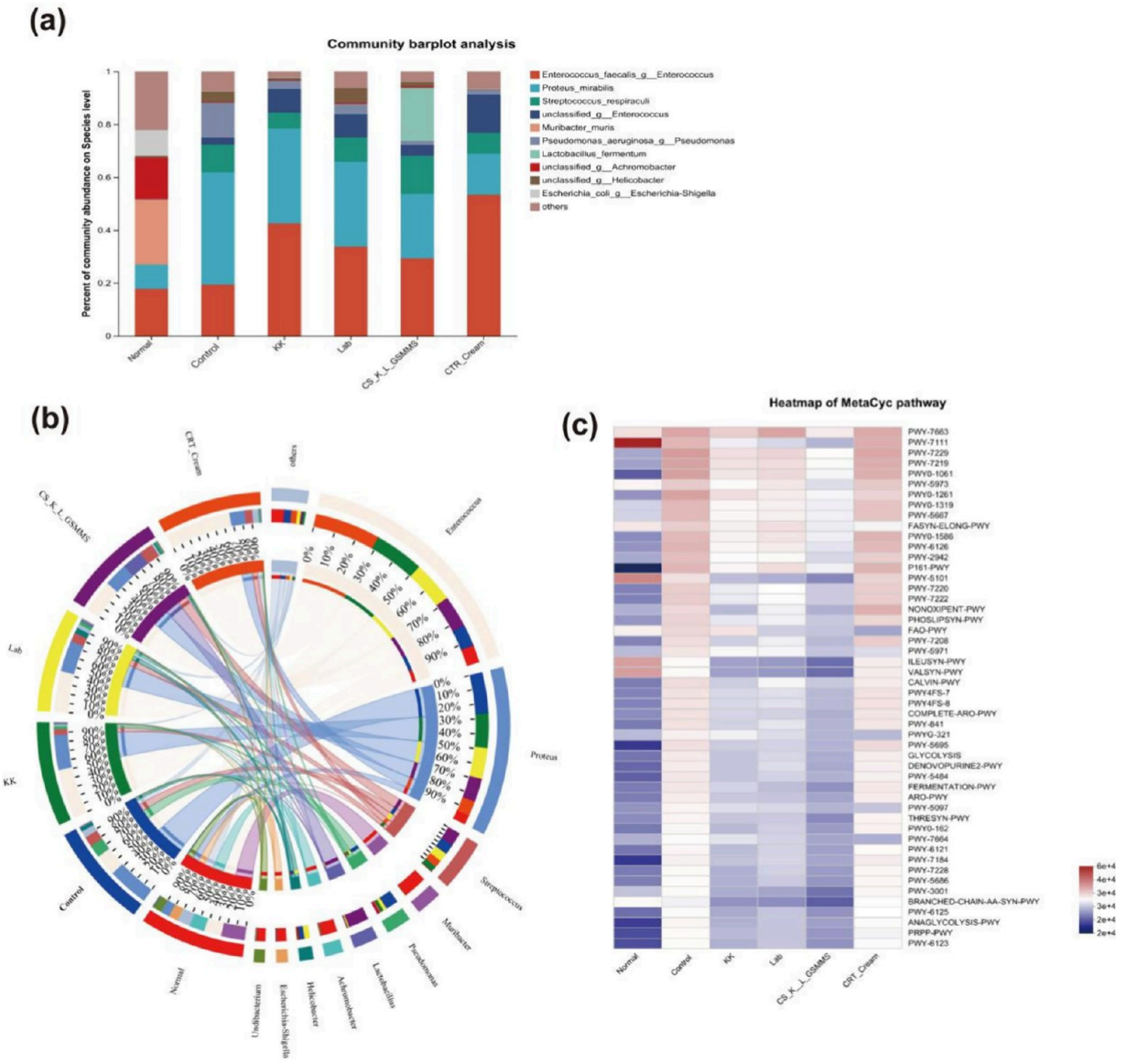

Figure 10. Microflora analysis after treatment with magnetic microspheres. (a) Community abundance percentage analysis on the species level. Flora analysis. (b) Circos sample and species relationship diagram circos sample and species relationship. (c) Species function prediction.

to obtain the mass of dry microspheres (M_1). The lyophilized microspheres were then immersed in SVF solution and incubated in a constant temperature shaker at 37 °C and 70 rpm. At various time intervals, the immersed microspheres were removed, and the mass (M_2) was measured after the surface water was absorbed by the filter paper. The solubilization ratio was calculated using eq 1.

$$\text{Swelling ratio} = \frac{(M_2 - M_1)}{M_1} \quad (1)$$

Lactobacillus Release. To determine the release of probiotics after encapsulation, 1 g of freshly prepared probiotic-loaded microspheres was divided into three portions. Each portion was added to 9 mL of SVF solution with KK concentrations of 0.16, 0.32, and 0.35 mg/mL, respectively, and incubated at 180 rpm in a constant-temperature incubation shaker at 37 °C. At the time points of 1, 2, 4, 8, 12, 20, and 24 h, 100 μL samples were taken. Test tubes were replenished with the same volume of the SVF solution at each time point. The removed culture solution was diluted, plated on MRS solid medium, and incubated in an anaerobic incubator overnight. The number of viable bacteria was counted, and the release curve was plotted. The experiment was repeated three times.

In Vitro AMP Release Profile. AMP-loaded magnetic gel microspheres (1 mg of drug per portion) were prepared. Three portions of these microspheres were added to each of three tubes containing 9 mL of SVF. All samples were placed in an incubation shaker at 37 °C and 70 rpm. At different time points, 200 μL of the solution was aspirated from each tube, and 200 μL of SVF was added to maintain a constant volume. Drug release was determined by measuring the drug content using the BCA protein assay, and cumulative drug-release-time curves were plotted for each group.

Model Construction and Treatment. All animal experiments were conducted in accordance with the regulations on the Administration of Laboratory Animals of China (revised in 2017). Eighty SPF-grade, 7-week-old female BALB/c mice, with a body mass of 18−20 g, were purchased from the Guangdong Medical Laboratory Animal Center. The mice were bred at the

https://doi.org/10.1021/acsomega.4c11016
ACS Omega 2025, 10, 11282−11295

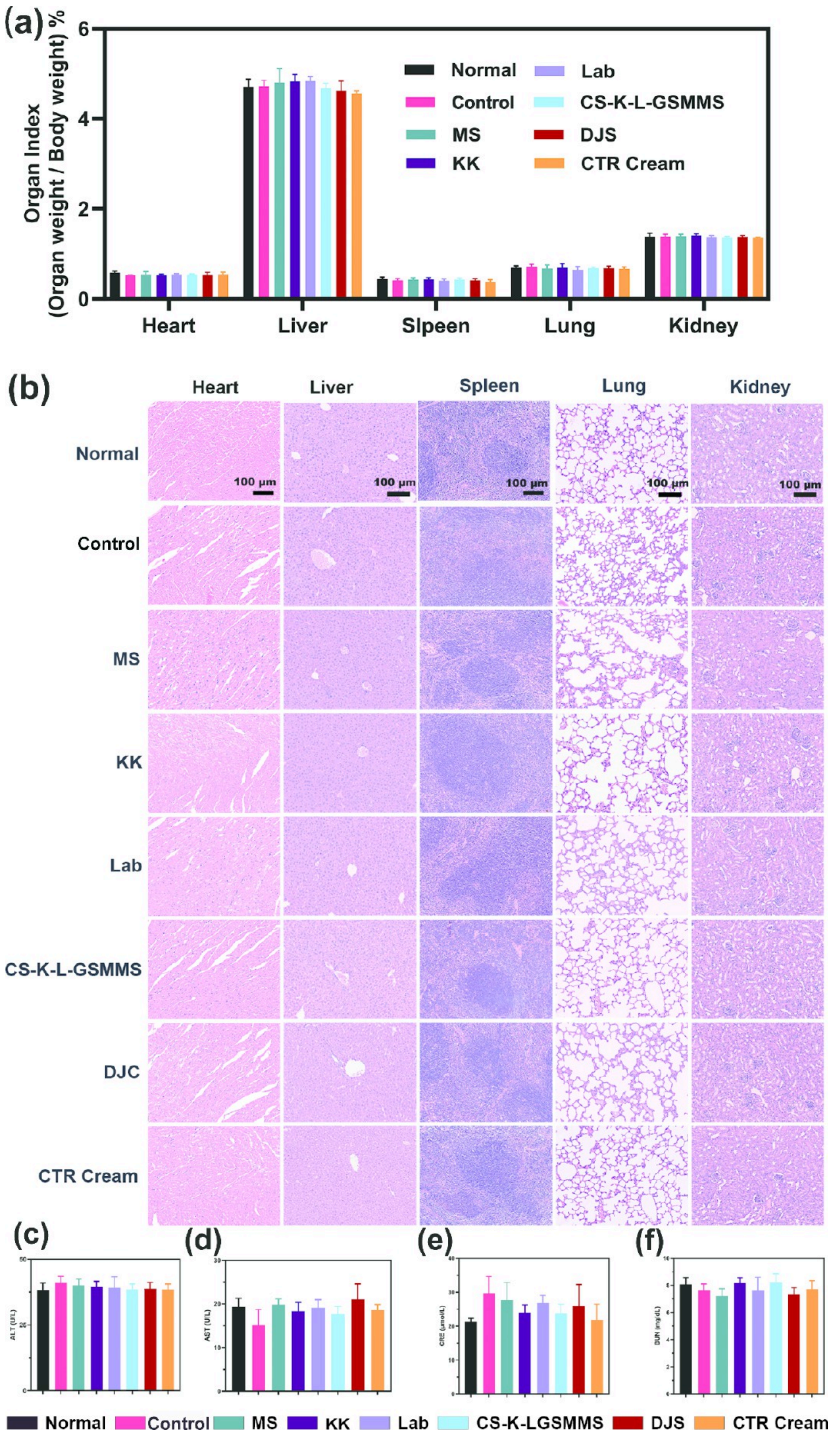

Figure 11. *In vivo* safety evaluation. (a) The effect of treatment on organ index in each group of mice. (b) H&E staining of heart, liver, spleen, lung, and kidney. (c–f) Liver and kidney function indicators: ALT (c), AST (d), CRE (e), and BUN (f).

Guangdong Pharmaceutical University Medical Laboratory Animal Centre (Laboratory Animal Use License SYXK (GD) 2022–0125). All experiments were performed in compliance with the laws and institutional guidelines related to animal ethics. A mouse vaginal model was performed similarly as described in Minooei.[38] Mice were randomly divided into eight groups. (n = 10).

Modeling: After 1 week of acclimatization, all mice except those in the normal group were injected subcutaneously with 0.1 mL of estradiol benzoate (2 mg/mL) to induce a pseudoestrus state. The injection was administered every other day. On the sixth day of injection, 100 μL of antibiotics at a concentration of 100 mg/mL was aspirated onto a sterile swab, which was then used to coat the vagina after the swab had fully absorbed the antibiotic. This treatment was administered six times over 2 days. The normal group was not treated. Following antibiotic treatment, 20 μL of *C. albicans* bacterial solution (approximately 5×10^4 CFU/ml bacteria) was inoculated into the vagina of the infected treatment group and the negative model control group of mice every day for a total of 5 days. Drug administration was discontinued for 1 day after successful modeling.

https://doi.org/10.1021/acsomega.4c11016
ACS Omega 2025, 10, 11282–11295

Table 1. Composition of the SVF

Reagents	Weighing volume (g/L)
NaCl	3.51
KOH	1.4
$Ca(OH)_2$	0.22
Bovine serum protein	0.018
Lactic acid	2
Acetic acid (CH_3COOH)	1
Glycerol	0.16
Urea $(NH_2)_2CO$	0.4
Glucose	5

Three mice from both the treatment group and the negative control group were randomly selected to collect vaginal secretions to confirm the success of the model. The secretions were examined microscopically, stained with PAS, and checked for mycelial spores.

Treatment: Following successful modeling, the mice were divided into the following groups: normal group (Normal), control group (Control), empty double-layer magnetic microsphere group (MS), CS-K-L-GSMMS group, live *lactobacillus* capsule for vaginal use group (DJS), and positive drug treatment group (CTR-Cream), with 10 mice in each group. Drug treatment was administered for 10 days. The control group was not treated, and blank microspheres were placed in the MS group once per day. The positive control groups included the positive drug group (using Clotrimazole cream) and *Lactobacillus* group (DJS), with the cream applied to the inside and surface of the vagina using a sterile cotton swab.

For the treatment groups, the KK group was injected with AMP KK, the *Lactobacillus* group was injected with *Lactobacillus* solution, and CS-K-L-GSMMS was placed in the vaginas of mice in this group. All treatments were administered once per day, except for the normal and modeling groups. During the treatment period, the affected area was observed and photographed, and body weight was recorded regularly. Every few days, three mice from each group were randomly selected to collect vaginal secretions. The vaginas were flushed with 0.9% NaCl injection (20 μL per time, for five consecutive times, totaling approximately 0.1 mL). A small amount of the secretion was used for microscopic examination, and the remaining volume was aspirated for dilution in a gradient, then coated on PDA agar culture plates and incubated at 28 °C. After 24 h, the cells were counted and photographed.

***In Vivo* Magnetic Residence Monitoring.** Six specific-pathogen-free female BALB/c mice were randomly selected and divided into two groups: a magnetic microsphere group (DiR-CS-K-L-GSMMS) and a magnetic microsphere-free group (DiR-CS-K-L-GSMS). The microspheres in both groups were labeled with fluorescent dyes and placed in the vaginas of the mice. Observation was conducted using a live imager in the vaginal area for 0, 6, 12, and 24 h. The fluorescence intensity of the microspheres was measured to determine their length of residence with mice anesthetized prior to the test.

Analysis of Changes in Fungal Load After Treatment. Vaginal irrigation fluid was collected at various time points. Then, 20 μL of sterile 0.9% NaCl solution was pipetted and used to rinse the vagina of the mice five times, totaling 0.1 mL. The sample was placed in a biosafety cabinet at a low temperature before further processing. The vaginal douching solution was diluted to 10^{-1}, 10^{-2}, and 10^{-3}, and coated onto PDA agar plates. These plates were incubated at 28 °C for 24 h. The following day, the plates were removed, counted, and photographed for preservation.

Histopathological Analysis of the Vagina. At the end of the experiment, the vaginal tissues from the mice were collected with excess fat and surface peritoneum removed. After treating tissue in 4% paraformaldehyde for 24 h, dehydrated and embedding in paraffin.[39] These sections were stained according to the instructions provided with the H&E staining kit and PAS staining kit.

Determination of Inflammatory Factors by ELISA. Each group received a 50−100 mg portion of vaginal tissue. After being crushed, lysed, homogenized, and underwent low-temperature centrifugation, the supernatant was collected. The supernatant was then analyzed according to the instructions for the use of the ELISA kits to detect pro-inflammatory factors TNF-α, IL-1β, IL-6, MIP-2, MCP-1, and the anti-inflammatory factor IL-4 in the vaginal tissue.

QPCR Determination of mRNA-Related Changes in Inflammatory Factors in Vaginal Tissue. Vaginal tissues were excised, weighed, and ground before further processing. The tissues weighing 80 mg were homogenized, and total RNA was extracted using 1 mL of Trizol reagent. qPCR was performed using the Evo M-MLV Reverse Transcription Premix Kit and SYBR Green Pro Taq HS Premix qPCR Kit according to the manufacturers' instructions.

Detection of Biomarkers of Oxidative Stress. All assays were performed according to the manufacturers' instructions for the respective kits: CAT using the ammonium molybdate colorimetric assay; SOD using the xanthine oxidase assay; and MDA using the thiobarbituric acid colorimetric assay.

Determination of Microflora Diversity in Vaginal Lavage Fluid Analysis. Vaginal secretions were collected by using a sterile 0.9% NaCl solution. The vaginal irrigation solution and secretions were stored at a low temperature and sent to the Meji Biological Co. Ltd. for processing and high-throughput sequencing.

***In Vivo* Safety Testing.** Organ Index and H&E Staining: All groups were fasted for 12 h before sampling, and the weight of the mice after fasting was determined (M). Mice were sacrificed by dislocation. All organs of the mice were collected, with excess tissues and fat removed. The surface of each organ was cleaned of residual blood with 0.9% NaCl solution, and the weight of each organ was recorded using an analytical balance (m) after moisture was removed with filter paper. The organ index was calculated as follows:

$$\text{Visceral index}\% = \frac{m}{M} \times 100\% \quad (2)$$

Additional organs (heart, liver, spleen, lungs, and kidneys) were collected from the mice, and each tissue was processed using the H&E staining method.

Liver and kidney function indexes: The mice were anesthetized with isoflurane, after which blood samples were collected from the orbital venous plexus and subsequently centrifuged to obtain the supernatant. Serum levels of AST, ALT, BUN, and CRE were determined using the respective index kits. The composition of the reagents and the experimental procedures were performed according to the instructions provided with the kits.

Statistical Analysis. Statistical analysis was performed using GraphPad Prism 9.0 (GraphPad Prism, San Diego, CA, USA). All data are presented as the mean ± the standard deviation.

https://doi.org/10.1021/acsomega.4c11016
ACS Omega 2025, 10, 11282−11295

Data analysis was conducted using one-way analysis of variance (ANOVA). Significance was demonstrated by $p < 0.05$.

■ ASSOCIATED CONTENT

Supporting Information

The Supporting Information is available free of charge at https://pubs.acs.org/doi/10.1021/acsomega.4c11016.

Histopathological changes in mice vaginal tissue, H&E and PAS staining results (Figure S1) (PDF)

■ AUTHOR INFORMATION

Corresponding Authors

Xuemei Lu − *Guangdong Provincial Key Laboratory of Pharmaceutical Bioactive Substances, School of Basic Medical Sciences, Guangdong Pharmaceutical University, Guangzhou 510006, People's Republic of China; Shenzhen Center for Disease Control and Prevention, Shenzhen 518055, People's Republic of China;* orcid.org/0000-0002-0571-1472; Phone: +86 02039352617; Email: luxuemei605@163.com

Shuiqing Gui − *Intensive Care Unit, Shenzhen Second People's Hospital, the First Affiliated Hospital of Shenzhen University, Shenzhen 518031, People's Republic of China*; Email: guishuiqing@163.com

Xiaobao Jin − *Guangdong Provincial Key Laboratory of Pharmaceutical Bioactive Substances, School of Basic Medical Sciences, Guangdong Pharmaceutical University, Guangzhou 510006, People's Republic of China*; Email: Jinxf2001@163.com

Yinghua Xu − *Key Laboratory of the Ministry of Health for Research on Quality and Standardization of Biotechnology Products, National Institutes for Food and Drug Control, Beijing 102629, People's Republic of China*; Email: xuyh@nifdc.org.cn

Authors

Haonan Li − *Guangdong Provincial Key Laboratory of Pharmaceutical Bioactive Substances, School of Basic Medical Sciences, Guangdong Pharmaceutical University, Guangzhou 510006, People's Republic of China; Shenzhen Center for Disease Control and Prevention, Shenzhen 518055, People's Republic of China; Intensive Care Unit, Shenzhen Second People's Hospital, the First Affiliated Hospital of Shenzhen University, Shenzhen 518031, People's Republic of China*

Huijuan Huang − *Guangdong Provincial Key Laboratory of Pharmaceutical Bioactive Substances, School of Basic Medical Sciences, Guangdong Pharmaceutical University, Guangzhou 510006, People's Republic of China; Shenzhen Center for Disease Control and Prevention, Shenzhen 518055, People's Republic of China; Intensive Care Unit, Shenzhen Second People's Hospital, the First Affiliated Hospital of Shenzhen University, Shenzhen 518031, People's Republic of China*

Sijia Xu − *Guangdong Provincial Key Laboratory of Pharmaceutical Bioactive Substances, School of Basic Medical Sciences, Guangdong Pharmaceutical University, Guangzhou 510006, People's Republic of China; Shenzhen Center for Disease Control and Prevention, Shenzhen 518055, People's Republic of China; Intensive Care Unit, Shenzhen Second People's Hospital, the First Affiliated Hospital of Shenzhen University, Shenzhen 518031, People's Republic of China*

Hongmei Tian − *Guangdong Provincial Key Laboratory of Pharmaceutical Bioactive Substances, School of Basic Medical Sciences, Guangdong Pharmaceutical University, Guangzhou 510006, People's Republic of China; Shenzhen Center for Disease Control and Prevention, Shenzhen 518055, People's Republic of China; Intensive Care Unit, Shenzhen Second People's Hospital, the First Affiliated Hospital of Shenzhen University, Shenzhen 518031, People's Republic of China*

Hui Xin − *Guangdong Provincial Key Laboratory of Pharmaceutical Bioactive Substances, School of Basic Medical Sciences, Guangdong Pharmaceutical University, Guangzhou 510006, People's Republic of China; Shenzhen Center for Disease Control and Prevention, Shenzhen 518055, People's Republic of China; Intensive Care Unit, Shenzhen Second People's Hospital, the First Affiliated Hospital of Shenzhen University, Shenzhen 518031, People's Republic of China*

Xuan Zou − *Shenzhen Center for Disease Control and Prevention, Shenzhen 518055, People's Republic of China*

Ziquan Lv − *Shenzhen Center for Disease Control and Prevention, Shenzhen 518055, People's Republic of China*

Xiangjie Yao − *Shenzhen Center for Disease Control and Prevention, Shenzhen 518055, People's Republic of China*

Complete contact information is available at: https://pubs.acs.org/10.1021/acsomega.4c11016

Notes

The authors declare no competing financial interest.

■ ACKNOWLEDGMENTS

This work was financially supported by the National Natural Science Foundation of China (No. 32070509, No. 82372161), the Guangdong Basic and Applied Basic Research Foundation (No. 2021A1515220119), the Shenzhen Science and Technology Program (No. JCYJ20220530150412027), the Shenzhen Fund for Guangdong Provincial High level Clinical Key Specialties (No. SZGSP006), the Sanming Project of Medicine in Shenzhen (No. SZSM202011008, No. SZSM202211016), and Shenzhen Key Medical Discipline Construction Fund (No. SZXK066).

■ REFERENCES

(1) Paladine, H. L.; Desai, U. A. Vaginitis: Diagnosis and Treatment. *American Family Physician* **2018**, *97* (5), 321−329.

(2) Gaziano, R.; Sabbatini, S.; Monari, C. The Interplay between Candida albicans, Vaginal Mucosa, Host Immunity and Resident Microbiota in Health and Disease: An Overview and Future Perspectives. *Microorganisms* **2023**, *11* (5), 1211.

(3) Li, H.; Miao, M.-x.; Jia, C.-l.; Cao, Y.-b.; Yan, T.-h.; Jiang, Y.-y.; Yang, F. Interactions between *Candida albicans* and the resident microbiota. *Frontiers in Microbiology* **2022**, *13*, DOI: 10.3389/fmicb.2022.930495.

(4) Gomaa, S. E.; Abbas, H. A.; Mohamed, F. A.; Ali, M. A. M.; Ibrahim, T. M.; Abdel Halim, A. S.; Alghamdi, M. A.; Mansour, B.; Chaudhary, A. A.; Elkelish, A.; et al. The anti-staphylococcal fusidic acid as an efflux pump inhibitor combined with fluconazole against vaginal candidiasis in mouse model. *BMC Microbiol* **2024**, *24* (1), 54.

(5) Sun, Z.; Ge, X.; Qiu, B.; Xiang, Z.; Jiang, C.; Wu, J.; Li, Y. Vulvovaginal candidiasis and vaginal microflora interaction: Microflora changes and probiotic therapy. *Front Cell Infect Microbiol* **2023**, *13*, 1123026.

(6) Gaziano, R.; Sabbatini, S.; Monari, C. The Interplay between, Vaginal Mucosa, Host Immunity and Resident Microbiota in Health and Disease: An Overview and Future Perspectives. *Microorganisms* **2023**, *11* (5), 1211.

(7) Sharma, K.; Parmanu, P. K.; Sharma, M. Mechanisms of antifungal resistance and developments in alternative strategies to combat *Candida albicans* infection. *Archives of Microbiology* **2024**, *206* (3). DOI: 10.1007/s00203-023-03824-1

(8) Witkin, S. S.; Forney, L. J. The microbiome and women's health: perspectives and controversies. *Bjog-an International Journal of Obstetrics and Gynaecology* **2020**, *127* (2), 127−127.
(9) Chen, X.; Lu, Y.; Chen, T.; Li, R. The Female Vaginal Microbiome in Health and Bacterial Vaginosis. *Frontiers in Cellular and Infection Microbiology* **2021**, *11*, DOI: 10.3389/fcimb.2021.631972.
(10) Saraf, V. S.; Sheikh, S. A.; Ahmad, A.; Gillevet, P. M.; Bokhari, H.; Javed, S. Vaginal microbiome: normalcy vs dysbiosis. *ARCHIVES OF MICROBIOLOGY* **2021**, *203* (7), 3793−3802.
(11) Ma, B.; Forney, L. J.; Ravel, J. Vaginal microbiome: rethinking health and disease. *Annu. Rev. Microbiol.* **2012**, *66*, 371−389.
(12) Muzny, C. A.; Laniewski, P.; Schwebke, J. R.; Herbst-Kralovetz, M. M. Host-vaginal microbiota interactions in the pathogenesis of bacterial vaginosis. *CURRENT OPINION IN INFECTIOUS DISEASES* **2020**, *33* (1), 59−65.
(13) Coppedge, N.; Garza, J.; Gandhi, K.; Sanchez, A.; Galloway, J.; Ventolini, G. *Lactobacillus* microbiota of the female genital tract in vaginal lactobacillosis. *ARCHIVES OF GYNECOLOGY AND OBSTETRICS* **2023**, *307* (5), 1319−1322.
(14) Novak, J.; Ravel, J.; Ma, B.; Ferreira, C. S. T.; Tristao, A. d. R.; Silva, M. G.; Marconi, C. Characteristics associated with *Lactobacillus* iners-dominated vaginal microbiota. *SEXUALLY TRANSMITTED INFECTIONS* **2022**, *98* (5), 353−359.
(15) Chee, W. J. Y.; Chew, S. Y.; Than, L. T. L. Vaginal microbiota and the potential of *Lactobacillus* derivatives in maintaining vaginal health. *Microbial Cell Factories* **2020**, *19* (1), DOI: 10.1186/s12934-020-01464-4.
(16) Wei, G.; Liu, Q.; Wang, X.; Zhou, Z.; Zhao, X.; Zhou, W.; Liu, W.; Zhang, Y.; Liu, S.; Zhu, C.; Wei, H. A probiotic nanozyme hydrogel regulates vaginal microenvironment for Candida vaginitis therapy. *Science Advances* **2023**, *9* (20), DOI: 10.1126/sciadv.adg0949.
(17) van Eijk, M.; Boerefijn, S.; Cen, L.; Rosa, M.; Morren, M. J. H.; van der Ent, C. K.; Kraak, B.; Dijksterhuis, J.; Valdes, I. D.; Haagsman, H. P.; et al. Cathelicidin-inspired antimicrobial peptides as novel antifungal compounds. *Med. Mycol* **2020**, *58* (8), 1073−1084.
(18) Li, X.; Zuo, S.; Wang, B.; Zhang, K.; Wang, Y. Antimicrobial Mechanisms and Clinical Application Prospects of Antimicrobial Peptides. *Molecules* **2022**, *27* (9), 2675.
(19) Buccini, D. F.; Cardoso, M. H.; Franco, O. L. Antimicrobial Peptides and Cell-Penetrating Peptides for Treating Intracellular Bacterial Infections. *Front Cell Infect Microbiol* **2021**, *10*, 612931.
(20) Duarte-Mata, D. I.; Salinas-Carmona, M. C. Antimicrobial peptideś immune modulation role in intracellular bacterial infection. *Front Immunol* **2023**, *14*, 1119574.
(21) Mba, I. E.; Nweze, E. I. Antimicrobial Peptides Therapy: An Emerging Alternative for Treating Drug-Resistant Bacteria. *Yale J. Biol. Med.* **2022**, *95* (4), 445−463.
(22) Mishra, B.; Lushnikova, T.; Golla, R. M.; Wang, X.; Wang, G. Design and surface immobilization of short anti-biofilm peptides. *Acta Biomater* **2017**, *49*, 316−328.
(23) Abbassi, F.; Lequin, O.; Piesse, C.; Goasdoué, N.; Foulon, T.; Nicolas, P.; Ladram, A. Temporin-SHf, a New Type of Phe-rich and Hydrophobic Ultrashort Antimicrobial Peptide. *J. Biol. Chem.* **2010**, *285* (22), 16880−16892.
(24) Wang, G.; Li, X.; Wang, Z. APD3: the antimicrobial peptide database as a tool for research and education. *Nucleic Acids Res.* **2016**, *44* (D1), D1087−1093.
(25) Myrovali, E. Hybrid Stents Based on Magnetic Hydrogels for Biomedical Applications. *ACS Appl. Bio Mater.* **2022**, *5* (6), 2598−2607.
(26) Wang, B.; Liu, D.; Liao, Y.; Huang, Y.; Ni, M.; Wang, M.; Ma, Z.; Wu, Z.; Lu, Y. Spatiotemporally Actuated Hydrogel by Magnetic Swarm Nanorobotics. *ACS Nano* **2022**, *16* (12), 20985−21001.
(27) Mollarasouli, F.; Zor, E.; Ozcelikay, G.; Ozkan, S. A. Magnetic nanoparticles in developing electrochemical sensors for pharmaceutical and biomedical applications. *Talanta* **2021**, *226*, 122108.
(28) Nowak-Jary, J.; Machnicka, B. Pharmacokinetics of magnetic iron oxide nanoparticles for medical applications. *J. Nanobiotechnology* **2022**, *20* (1), 305.
(29) Tang, J.; Yao, C.; Gu, Z.; Jung, S.; Luo, D.; Yang, D. Super-Soft and Super-Elastic DNA Robot with Magnetically Driven Navigational Locomotion for Cell Delivery in Confined Space. *Angew. Chem., Int. Ed. Engl.* **2020**, *59* (6), 2490−2495.
(30) Zeng, N.; He, L.; Jiang, L.; Shan, S.; Su, H. Synthesis of magnetic/pH dual responsive dextran hydrogels as stimuli-sensitive drug carriers. *Carbohydr. Res.* **2022**, *520*, 108632.
(31) Cirri, M.; Maestrelli, F.; Scuota, S.; Bazzucchi, V.; Mura, P. Development and microbiological evaluation of chitosan and chitosan-alginate microspheres for vaginal administration of metronidazole. *Int. J. Pharm.* **2021**, *598*, 120375.
(32) Liu, J.; Liu, F.; Ren, T.; Wang, J.; Yang, M.; Yao, Y.; Chen, H. Fabrication of fish gelatin/sodium alginate double network gels for encapsulation of probiotics. *J. Sci. Food Agric* **2021**, *101* (10), 4398−4408.
(33) Yang, J.; Yao, J.; Wang, S. Electromechanical response performance of a reinforced biomass gel artificial muscle based on natural polysaccharide of sodium alginate doped with an ionic liquid for micro-nano regulation. *Carbohydr. Polym.* **2022**, *275*, 118717.
(34) Shi, H.; Huang, Y.; Cheng, C.; Ji, G.; Yang, Y.; Yuan, H. Preparation and characterization of chain-like and peanut-like Fe3O4@SiO2 core-shell structure. *J. Nanosci Nanotechnol* **2013**, *13* (10), 6953−6960.
(35) Guo, Y. Development and Evaluation of an Intelligent Magnetic Actuated Probiotic M.P-KGM/SA Gel for the Improvement of Constipation [D] Guangdong Pharmaceutical University, Guangzhou, 2023.
(36) Srivastava, M.; Singh, J.; Yashpal, M.; Gupta, D. K.; Mishra, R. K.; Tripathi, S.; Ojha, A. K. Synthesis of superparamagnetic bare Fe_3O_4 nanostructures and core/shell (Fe_3O_4/alginate) nanocomposites. *Carbohydr. Polym.* **2012**, *89* (3), 821−829.
(37) Owen, D. H.; Katz, D. F. A vaginal fluid simulant. *Contraception* **1999**, *59* (2), 91−95.
(38) Mo, H.; Zhang, T.; Zhang, J.; Peng, S.; Xiang, F.; Li, H.; Ge, Y.; Yao, L.; Hu, L. Ferrous sulphate triggers ferroptosis in *Candida albicans* and cures vulvovaginal candidiasis in a mouse model. *Microbiol Res.* **2024**, *283*, 127704.
(39) Manolea, M. M.; Istrate-Ofiţeru, A. M.; Săndulescu, M. S.; Camen, I. V.; Piciu, I. A.; Dijmărescu, A. L.; Vrabie, S. C.; Neamţu, S. D.; Obleagă, C. V.; Siminel, M. A. Clinical and morphopathological assay in vulvovaginal candidiasis. *Rom J. Morphol Embryol* **2023**, *63* (3), 511−520.

https://doi.org/10.1021/acsomega.4c11016
ACS Omega 2025, 10, 11282−11295